

# Novel Entries in a Fungal Biofilm Matrix Encyclopedia

Robert Zarnowski,<sup>a</sup> William M. Westler,<sup>b</sup> Ghislain Ade Lacmbouh,<sup>c</sup> Jane M. Marita,<sup>d</sup> Jameson R. Bothe,<sup>c</sup> Jörg Bernhardt,<sup>e,f</sup> Anissa Lounes-Hadj Sahraoui,<sup>g</sup> Joël Fontaine,<sup>g</sup> Hiram Sanchez,<sup>a</sup> Ronald D. Hatfield,<sup>d</sup> James M. Ntambi,<sup>c,h</sup> Jeniel E. Nett,<sup>a,i</sup> Aaron P. Mitchell,<sup>j</sup> David R. Andes<sup>a,i</sup>

Department of Medicine, Infectious Diseases, University of Wisconsin, Madison, Wisconsin, USA<sup>a</sup>; National Magnetic Resonance Facility at Madison, University of Wisconsin, Madison, Wisconsin, USA<sup>b</sup>; Department of Biochemistry, University of Wisconsin, Madison, Wisconsin, USA<sup>c</sup>; Dairy Forage Research Center, U.S. Department of Agriculture, Madison, Wisconsin, USA<sup>d</sup>; Universität Institute for Microbiology, Ernst Moritz Arndt University, Greifswald, Germany<sup>e</sup>; DECODON GmbH, BioTechnikum Greifswald, Germany<sup>f</sup>; Université du Littoral Côte d'Opale, Unité de Chimie Environnementale at Interactions sur le Vivant, Calais, France<sup>g</sup>; Department of Food Sciences, University of Wisconsin, Madison, Wisconsin, USA<sup>h</sup>; Department of Medical Microbiology and Immunology, University of Wisconsin, Madison, Wisconsin, USA<sup>i</sup>; Biological Sciences, Carnegie Mellon University, Pittsburgh, Pennsylvania, USA<sup>j</sup>

**ABSTRACT** Virulence of *Candida* is linked with its ability to form biofilms. Once established, biofilm infections are nearly impossible to eradicate. Biofilm cells live immersed in a self-produced matrix, a blend of extracellular biopolymers, many of which are uncharacterized. In this study, we provide a comprehensive analysis of the matrix manufactured by *Candida albicans* both *in vitro* and in a clinical niche animal model. We further explore the function of matrix components, including the impact on drug resistance. We uncovered components from each of the macromolecular classes (55% protein, 25% carbohydrate, 15% lipid, and 5% nucleic acid) in the *C. albicans* biofilm matrix. Three individual polysaccharides were identified and were suggested to interact physically. Surprisingly, a previously identified polysaccharide of functional importance,  $\beta$ -1,3-glucan, comprised only a small portion of the total matrix carbohydrate. Newly described, more abundant polysaccharides included  $\alpha$ -1,2 branched  $\alpha$ -1,6-mannans (87%) associated with unbranched  $\beta$ -1,6-glucans (13%) in an apparent mannan-glucan complex (MGCx). Functional matrix proteomic analysis revealed 458 distinct activities. The matrix lipids consisted of neutral glycerolipids (89.1%), polar glycerolipids (10.4%), and sphingolipids (0.5%). Examination of matrix nucleic acid identified DNA, primarily noncoding sequences. Several of the *in vitro* matrix components, including proteins and each of the polysaccharides, were also present in the matrix of a clinically relevant *in vivo* biofilm. Nuclear magnetic resonance (NMR) analysis demonstrated interaction of aggregate matrix with the antifungal fluconazole, consistent with a role in drug impedance and contribution of multiple matrix components.

**IMPORTANCE** This report is the first to decipher the complex and unique macromolecular composition of the *Candida* biofilm matrix, demonstrate the clinical relevance of matrix components, and show that multiple matrix components are needed for protection from antifungal drugs. The availability of these biochemical analyses provides a unique resource for further functional investigation of the biofilm matrix, a defining trait of this lifestyle.

Received 14 May 2014 Accepted 10 July 2014 Published 5 August 2014

**Citation** Zarnowski R, Westler WM, Lacmbouh GA, Marita JM, Bothe JR, Bernhardt J, Lounes-Hadj Sahraoui A, Fontaine J, Sanchez H, Hatfield RD, Ntambi JM, Nett JE, Mitchell AP, Andes DR. 2014. Novel entries in a fungal biofilm matrix encyclopedia. *mBio* 5(4):e01333-14. doi:10.1128/mBio.01333-14.

**Invited Editor** Jose Lopez-Ribot, The University of Texas at San Antonio (UTSA) **Editor** Judith Berman, University of Minnesota, GCD

**Copyright** © 2014 Zarnowski et al. This is an open-access article distributed under the terms of the [Creative Commons Attribution-Noncommercial-ShareAlike 3.0 Unported license](https://creativecommons.org/licenses/by-nc-sa/4.0/), which permits unrestricted noncommercial use, distribution, and reproduction in any medium, provided the original author and source are credited.

Address correspondence to David R. Andes, dra@medicine.wisc.edu.

In the microbial world, existence within surface-associated multicellular communities is exceedingly common (1, 2). In fact, most microorganisms appear capable of forming biofilms. In the medical arena, it is argued that this lifestyle is responsible for the great majority of human infections (3). Biofilms share an important structural feature: their constituent cells are encased within and bound by an extracellular matrix (4, 5). The composition of the matrix varies among microbial biofilms but often consists of a combination of macromolecules, including polysaccharides, proteins, nucleic acids, and lipids. As a characteristic feature of biofilms, the extracellular matrix has been shown to provide numerous functions, including cellular cohesion, community structure, nutritional resource, and protection from xenobiotics, antimicrobials, and the host immune system.

*Candida albicans* is the most common hospital-associated fun-

gal pathogen and frequently produces biofilm infection of medical devices, resulting in the highest mortality among nosocomial pathogens (6, 7). Previous work has identified a prominent role for the *Candida* matrix in development of the drug-resistant phenotype associated with the biofilm mode of growth. This material has been shown to sequester antifungals, and molecular studies have linked  $\beta$ -1,3-glucan, an extracellular carbohydrate, to this process (8–14). However, the relatively low concentration of this matrix polysaccharide compared to extracellular drug concentrations suggested that other biofilm matrix components may very well be involved in the matrix sequestration of antifungals. To address this knowledge gap, we initiated a biochemical analysis of the extracellular matrix of biofilms produced by *C. albicans*. We reasoned that this endeavor would not only help to identify additional antifungal-sequestering matrix components but would also

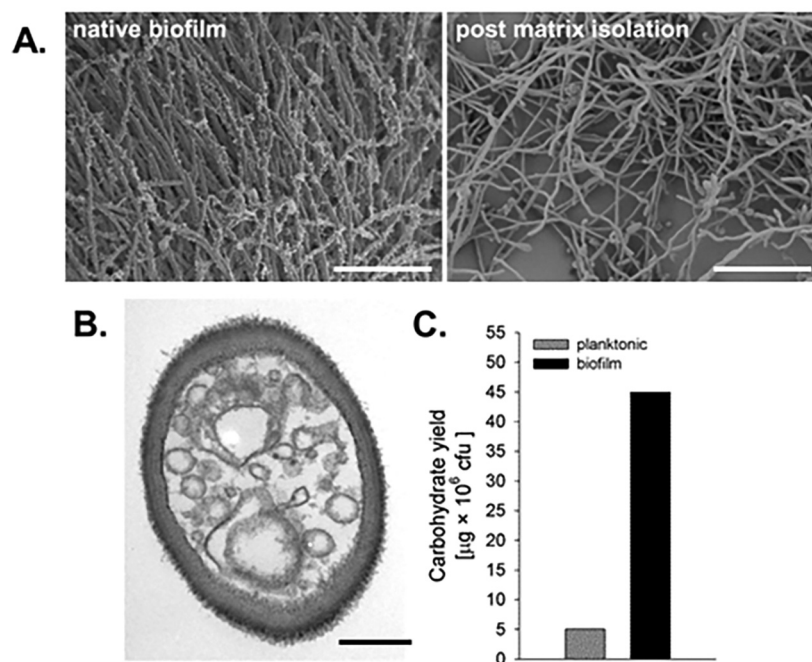


**FIG 1** Impact of the matrix isolation process on *C. albicans* biofilm and planktonic cells. (A) The matrix collection process visibly removes matrix, leaving fungal cells intact based upon scanning electron microscopy (SEM) of the biofilm pre- and postcollection. The scale bar represents 50  $\mu\text{m}$ . (B) The matrix collection process does not visibly impact the cell wall of fungi based upon TEM of postcollection cells. The scale bar represents 1  $\mu\text{m}$ . (C) The matrix processing does not extract cell wall components from planktonic (nonbiofilm) cells.

serve as a resource for laboratories investigating various aspects of fungal biofilms. Here, we present a comprehensive biochemical analysis of *C. albicans* biofilm matrix. Unique components from each macromolecular category were identified and characterized. The presence of many of these components was also confirmed using *in vivo* models of biofilm infection. Finally, by employing nuclear magnetic resonance (NMR) to analyze intact and individual matrix fractions, we identified a matrix-antifungal interaction that appears to require cooperation of several fungus-derived elements.

## RESULTS

**Macromolecular composition of *Candida albicans* biofilm matrix.** Using a large-scale, roller bottle apparatus for *Candida* biofilm production, we collected an average biofilm dry biomass density of 146.7  $\mu\text{g}/\text{cm}^2$ . To ensure the isolation and processing method did not promote cell leakage or cell damage, we assessed cell wall composition using transmission electron microscopy (TEM) and biochemical assays. As shown in Fig. 1, this step detached the matrix from fungal cells but did not appreciably remove the cell wall components of biofilm or planktonic cells. Each of the four macromolecular components was represented in the biofilm matrix, including proteins and their glycosylated counterparts (55% [wt/wt]), carbohydrates (~25% [wt/wt]), lipids (~15% [wt/wt]), and deoxyribonucleic acids (~5% [wt/wt]).

**Identification of the matrix mannan-glucan complex.** Complementary biochemical and imaging analyses of the matrix polysaccharide identified a series of two previously unidentified neutral polysaccharides in the biofilm matrix. The most abundant components were an  $\alpha$ -1 $\rightarrow$ 6-linked mannan and  $\alpha$ -1 $\rightarrow$ 2-linked side chains that appeared complexed to linear  $\beta$ -1,6-glucan, a mannan-glucan complex (MGCx).

Monosugar analysis of the total biofilm matrix revealed four relatively abundant monosaccharides, arabinose (Ara), mannose (Man), glucose (Glc), and xylose (Xyl), which accounted for 47.9%, 20%, 12.5%, and 12.6% of the total carbohydrate pool. Initial size exclusion chromatography of the crude matrix yielded two major pools: a high-molecular-weight (HMW) fraction and low-molecular-weight (LMW) fraction that contained 38.3% and 61.7% of the matrix material, respectively (Fig. 2A). Of the total matrix carbohydrates, 27.1% separated in the LMW pool, which contained mostly Ara (52.2%) with smaller amounts of Man, Xyl, and Glc (13.8%, 13.8%, and 12.9%, respectively). The HMW pool contained 21.6% of the total carbohydrate and consisted primarily of Man (89.2%) and Glc (8.6%).

The neutral polysaccharides from the HWM pool were chosen for further structural analysis based upon assumed likelihood of structural complexity and function (Fig. 2B). The HMW component was separated into 22 fractions based upon size (Fig. 2C). The molecular weights of polysaccharide fractions varied from 247.2 to 4.2 (Fig. 2D). Six of the 22 carbohydrate fractions (F2, F5, F10, F14, F16, and F17) in the neutral HMW fraction were selected based upon size variation and abundance for nuclear magnetic resonance (NMR) and gas chromatography (GC) linkage studies.  $^1\text{H}$  NMR-based comparative analysis of the lower-molecular-weight F10, F14, F16, and F17 fractions demonstrated identical NMR spectra, suggesting they belonged to the same polysaccharide homologue series (Fig. 2E). Monosugar analysis of these polysaccharides showed a composition of 85% Man and 15% Glc. This ratio of monosaccharides remained relatively constant among the fractions, consistent with either the simultaneous coelution of both sugar homologues or the existence of distinct single mannan-glucan complex polysaccharides in the *C. albicans* biofilm matrix.

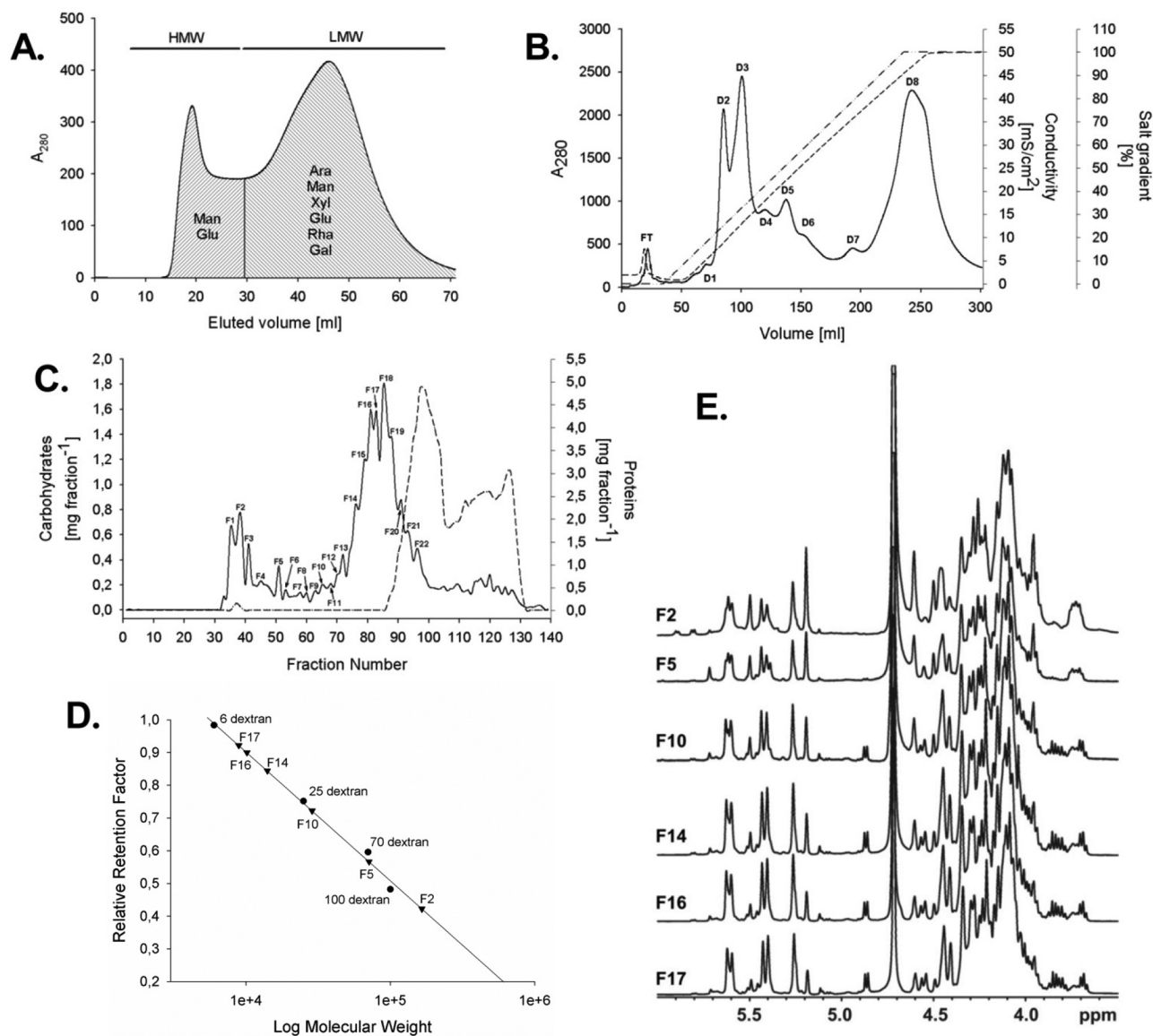


**FIG 2** Chromatographic fractionation and NMR analysis of carbohydrates from the *C. albicans* biofilm extracellular matrix. (A) Initial fractionation employing flash size exclusion chromatography on the HiPrep 26/10 Desalting Sephadex G-25 Fine column. The matrix sample was separated into the Man/Glc-rich HMW fraction (38.3%) and the Ara-rich LMW fraction (61.7%). Proteins were detected at 280 nm. (B) Fractionation of the HMW fraction on the weak anion exchanger HiPrep 16/10 DEAE FF column resulted in separation of uncharged protein-free polysaccharides from charged proteins and glycoproteins. Polysaccharides were eluted in the flowthrough fraction (shown as FT), whereas multiple (glyco) protein peaks, D1 to D8, were separated in the applied salt gradient (dashed line with larger spaces) as reflected by increasing conductivity (dashed line with smaller spaces). (C) Purification of neutral polysaccharides in gel filtration chromatography on the HighPrep 16/60 Sephacryl S-300 HR column. This procedure yielded a total of 22 individual polysaccharide-positive peaks, F1 to F22. (D) Size exclusion column calibration with a set of *Leuconostoc* species dextran standards at the following molecular weights: 100, 70, 40, 25, and 6. Positions of the select purified polysaccharides, F2, F5, F10, F14, F16, and F17, are indicated by reverse triangles. (E) Comparison of the 500-MHz  $^1\text{H}$  NMR spectra of representative purified matrix neutral polysaccharides, F2, F5, F10, F14, F16, and F17, from the *C. albicans* biofilm matrix.

To consider these possibilities, we elected to use a combination of one-dimensional (1D) and 2D NMR for the two most abundant fractions. This analysis also identified two major structural mannosyl and glucosyl motifs suggestive of an MGCx (Fig. 3) (15–20). Table S1 in the supplemental material lists the assignments of spin systems and relative abundance found in each sample.

The NMR spectra of F17 polymers revealed several  $\alpha$ - and  $\beta$ -Man spin systems and two  $\beta$ -Glu spin systems (Fig. 3A and B). The major polysaccharide was consistent with a backbone of  $\alpha$ -1 $\rightarrow$ 6-linked mannan and  $\alpha$ -1 $\rightarrow$ 2-linked side chains. This

would account for the presence of 2,6-Man residues that were 1 $\rightarrow$ 6 linked to 6-Man or to 2,6-Man, as well as the absence of 6-Man that was 1 $\rightarrow$ 2 linked to either 2-Man or 2,6-Man. Based on relative abundance, it appeared that every second or third backbone Man residue was substituted with a side chain averaging 2 to 3 Man residues long. In total, these side chains accounted for approximately 10.5% of  $\beta$ -Man residues. After the matrix mannan polysaccharide, the next most abundant polysaccharide identified was  $\beta$ -1,6-glucan. Linkage analysis suggested that the  $\beta$ -1,6-glucan consisted of residues solely in a linear form. Surprisingly,



$\beta$ -1,3-glucan was not found in the free (neutral) fraction by NMR methods but was identified in the glycoprotein fraction using the GlucateLL assay as previously described (10, 14). Interestingly, the NOESY (nuclear Overhauser effect spectroscopy) and HMBC (heteronuclear multiple-bond correlation spectroscopy) did not identify an obvious linkage between glucan and mannan residues via NMR. However, the uniform identification of mannosyl and glucosyl residues (GMCx) with a constant ratio in each of the chromatographic fractions is consistent with a physical association.

The NMR spectra of F2 revealed only  $\alpha$ - and  $\beta$ -Man spin systems and no evidence of glucan (Fig. 3C and D; see also Table S1 in the supplemental material). However, GC monosugar analysis demonstrated the presence of glucose (4%). We speculate the lack of NMR signature may be due to the relatively low concentrations of this polymer in the sample. The majority of mannan spin systems were comparable to those observed in the higher-molecular-weight fractions, suggesting structural similarities. However, F2 contained more  $\beta$ -Man residues (33.6%) than the F17 fraction (10.5%), and those residues were located primarily in 1,2-linked side chains. F2 also contained almost 10 times more Man-1-phosphate residues than F17. These groups were linked either via  $\alpha$ -1,2 or  $\beta$ -1,2 bonds, and the latter type was not detected in F17 mannan. These composite results demonstrate the F2 fraction consists of a high-molecular-weight mannan with increased length of side chains and unique Man-1P residues.

Small-angle X-ray scattering (SAXS) was used to gain further insight into the molecular size and shape of the most abundant mannan polysaccharide. The SAXS-derived molecular shape was consistent with the mannan side chain distribution proposed in Fig. 3F to H, specifically, a model of a mannan chain (molecular weight of 6.8) with  $\alpha$ -1,2 linkage lengths alternating between 2 and 3 mannosyl residues. An overlay of the average molecular shape and atomic model shown in Fig. 3G demonstrates congruence. While the mannan chains are highly flexible and contain heterogeneous side chain distributions, the static model in Fig. 3H shows that the proposed side chain distributions represent a reasonable model estimate.

Confocal imaging of *in vitro* biofilms was undertaken to examine the distribution of mannan and  $\beta$ -1,6-glucan matrix components by labeling with monoclonal antibodies developed against and specific for purified matrix components (data not shown). The images demonstrated an extracellular location for each polysaccharide and a distribution throughout the biofilm depth in Fig. 4A to C. The two-channel image color is suggestive of polysaccharide colocalization and consistent with an MGCx (Fig. 4D).

As environmental and host conditions have been shown to impact biofilm extent and composition, we sought to identify the clinical significance of the *in vitro* biofilm biochemical analyses via exploration in a relevant *in vivo* model. Imaging of intact rat catheter-associated biofilms using anti-mannan and anti- $\beta$ -1,6-glucan-labeled antibodies raised against purified matrix compo-

nents showed extracellular staining throughout the biofilm thickness (Fig. 4E to G). The distribution was similar to that observed in the *in vitro* model. Immuno-TEM of biofilm scraped from the catheter model identified matrix  $\beta$ -1,3-glucan using gold particle-labeled antibodies. The  $\beta$ -1,3-glucan was sparsely scattered throughout the extracellular matrix, consistent with the modest concentration of this polysaccharide relative to that of other components (Fig. 4H).

**Lipid analysis of *C. albicans* biofilm matrix.** Lipid analysis using gas chromatography identified eight different classes of lipids in the matrix. The matrix lipid profile included predominantly glycerolipids (99.5%) with a small portion of sphingolipids (0.5%) (see Table S2 in the supplemental material). Neutral glycerolipids constituted 89.2%, while polar glycerolipids were less abundant (10.4%). The majority of glycerolipids consisted of neutral classes of free fatty acids and triacylglycerols, as well as other polar phosphatidylethanolamines. Thirteen different fatty acid side chains were identified on these lipids (see Table S2). The most abundant fatty acids were oleic acid (18:1) and linoleic acid (18:2), which comprised 86.9% and 76.4% of the total fatty acid pool, respectively. Palmitic acid (16:0), stearic acid (18:0), palmitoleic acid (16:1), and myristic acid (14:0) were present in smaller amounts.

Phosphatidylethanolamine was the most abundant class of polar glycerolipids in the matrix. This group of lipids consisted mostly of palmitoleic acid (31.5%) and almost equal amounts of palmitic and oleic acids (26.4 and 26.1%, respectively). Fatty acid patterns measured in two other polar glycerolipid classes, phosphatidylserine and phosphatidylinositol, were highly similar and contained palmitic, stearic, and oleic acids. Phosphatidylcholine was the only group of polar glycerolipids that contained arachidonic acid at a relatively modest concentration (3.3%). A precursor of eicosanoids, prostaglandin  $E_2$ , was also found in small amounts in the matrix lipid sample using mass spectrometry (MS) (see Fig. S1 in the supplemental material). Ergosterol (ergosta-5,7,22-trien-3 $\beta$ -ol) was the only sterol identified in MS analyses, and its quantity was modest at 70 ng/mg of the matrix.

**Proteomic analysis of biofilm matrix.** By mass spectrometry, a total of 565 proteins were identified in the *C. albicans* biofilm matrix. The KEGG Ontology ID database discerned 458 different functions (see Table S3 in the supplemental material). The visualization of relative quantities of biofilm matrix proteins was also performed using KEGG protein functional categorization. On the basis of this hierarchical classification scheme, Voronoi treemaps were also constructed (21). This approach divides screen space according to hierarchy levels where main functional categories determine screen sections on the first level, subsidiary categories on the second level, and so forth. The polygonic cells of the deepest level represented functionally classified matrix proteins and were colored according to relative abundance of each protein that was determined based on total counts of corresponding trypsin-digested peptides.

#### Figure Legend Continued

continuing on average 3 to 4 mannosyl residues. (F) Predicted structures of the *C. albicans* biofilm matrix neutral polysaccharides:  $\alpha$ -1,2 branched  $\alpha$ -1,6-mannans,  $\beta$ -1,6- and  $\beta$ -1,3-glucans. G and M denote glucan and mannan, whereas HMW and LMW refer to high- and low-molecular-weight polysaccharide homologue series, respectively. Values in parentheses represent a percentage content of each sugar type in the total neutral polysaccharide pool in the matrix. (G) SAXS 1D scattering profiles for the F20 (black) and F21 (red) fractions. (H) Average low-resolution dummy atom model of F20 (green) generated from 20 independent DAMMIF runs overlaid with a mannan with a molecular weight of 6.8 (blue) that has the branching distributions proposed in the legend to panel F.

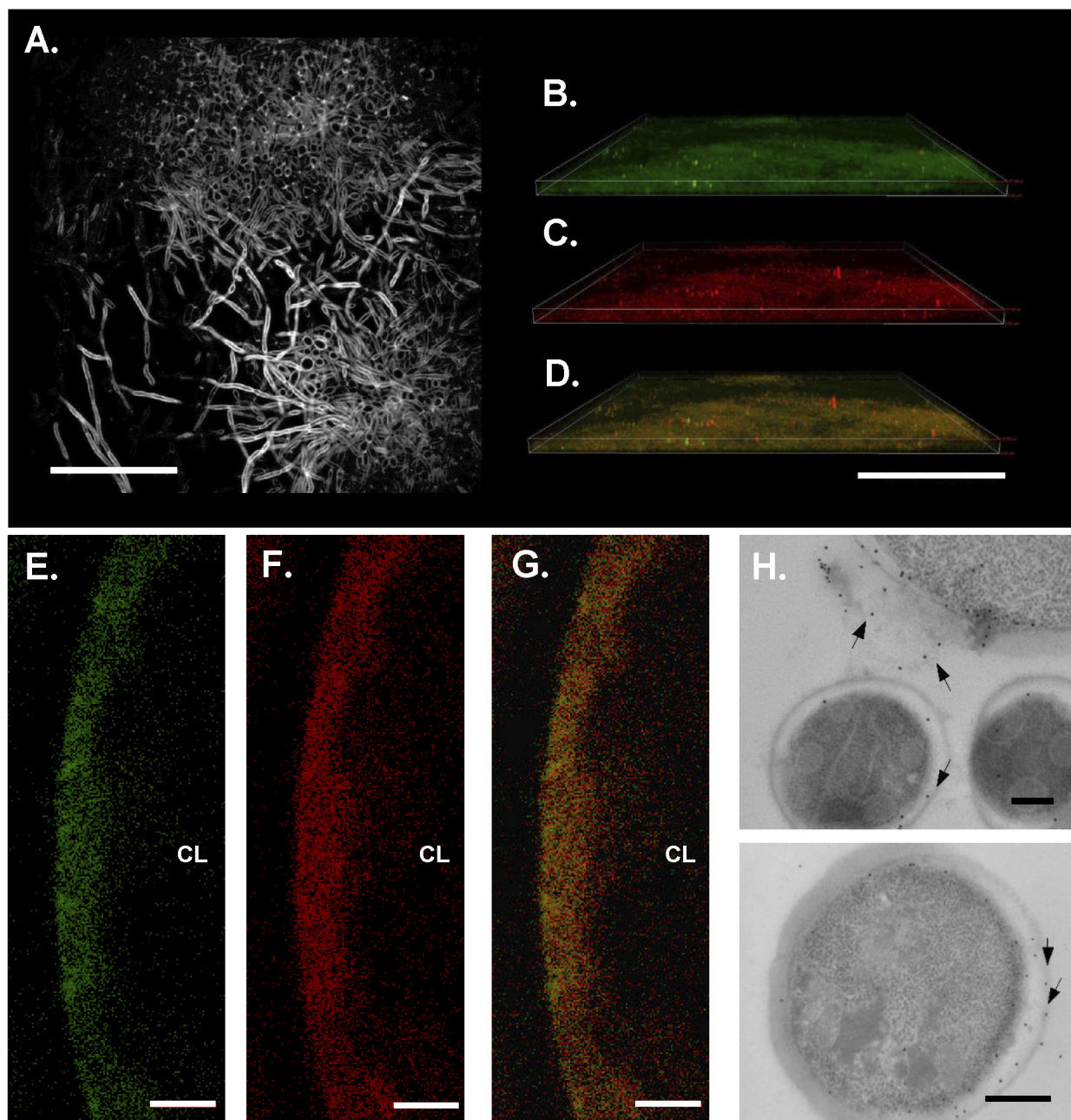


**FIG 4** Detection of  $\alpha$ -1,2 branched  $\alpha$ -1,6-mannan,  $\beta$ -1,6-glucan, and  $\beta$ -1,3-glucan in the *C. albicans* biofilm matrix using an *in vitro* biofilm model (A to D) and the *in vivo* rat catheter biofilm model (E to H). The scale bars in panels A, E, F, and G are 50  $\mu$ m. (A) *In vitro* biofilm community of yeast and hyphae visualized using a calcofluor white stain. (B) Detection of  $\alpha$ -1,2 branched  $\alpha$ -1,6-mannan in the *in vitro* biofilm matrix using anti- $\alpha$ -1,2 branched  $\alpha$ -1,6-mannan monoclonal antibody fluorescently labeled with FITC. (C) Detection of  $\beta$ -1,6-glucan in the *in vitro* biofilm matrix using anti- $\beta$ -1,6-glucan monoclonal antibody fluorescently labeled with rhodamine. (D) An overlay of both stains showed extracellular staining throughout the *in vitro* biofilm thickness, and the yellow color is consistent with colocalization. The scale bar is 200  $\mu$ m. (E) Detection of  $\alpha$ -1,2 branched  $\alpha$ -1,6-mannan in the *in vivo* rat catheter biofilm matrix. CL indicates catheter lumen. (F) Detection of  $\beta$ -1,6-glucan in the *in vivo* rat catheter biofilm matrix. (G) An overlay of both stains showed extracellular staining throughout the biofilm thickness. (H) Immuno-TEM of biofilm scraped from the catheter model identified  $\beta$ -1,3-glucan using gold particle-labeled antibodies. As indicated by arrows,  $\beta$ -1,3-glucan was sparsely scattered throughout the extracellular matrix, consistent with the modest concentration of this polysaccharide relative to other components. The scale bar is 0.5  $\mu$ m.

The putative function of the largest number of proteins involved metabolism and included 16 metabolic pathways (see Fig. S2A in the supplemental material). The most abundant (20%) were from pathways related to carbohydrate, amino acid, and energy metabolism pathways (see Fig. S2B). Among these, 177 func-

tional proteins representing the carbohydrate metabolism supergroup were identified, which constituted 50.4% of all of the *C. albicans* proteins annotated in this category (351 proteins). These proteins could be further assigned into 14 distinct metabolic pathways, and the most abundant clusters included the citric

acid cycle (30 proteins), the pyruvate metabolism pathway (28 proteins), and the glycolysis/gluconeogenesis pathway (19 proteins). Amino acid metabolism was represented by 136 enzymatic proteins, which constituted 41.3% of a total 329 annotated proteins in this supergroup. These could be additionally classified into 13 distinct metabolic pathways that represented the vast majority of essential and nonessential amino acid anabolic and catabolic processes. A single nonmetabolic protein, heat shock protein (Hsp70), had been detected in other matrix and biofilm analyses. Search of ontology in the *Candida* Genome Database revealed that 8 of the 280 currently identified matrix proteins had previously been reported to impact biofilm formation or function (Xog1, Exg1, Bgl2, Pmt1, Pmt2, Pmt4, Pmt6, Hsp70) (13, 22). With the exception of Hsp70, each would be predicted to impact the production or modification of polysaccharides found in the matrix.

Matrix proteins were also collected from three clinical biofilm niches using rodent models which closely mimic human biofilm infections on medical devices (intravenous central catheter, urinary catheter, and denture). On proteomic analysis, the majority of proteins identified in each model were of mammalian origin. Only 16 *C. albicans* proteins were identified among the *in vivo* models (see Table S4 in the supplemental material). All but three proteins from this *in vivo* group were also identified in the *in vitro* biofilm system. Similar to *in vitro* conditions, other than the Hsp70 family heat shock protein, the putative function of each matrix protein was related to metabolism.

**Matrix nucleic acid composition.** The presence of extracellular DNA (eDNA) has been described in *C. albicans* biofilms (23), but limited information regarding the nature of this biopolymer is available. Upon examining the DNA sequence relative to available libraries, we found the matrix DNA to be almost exclusively composed of random noncoding sequences. Fifteen selected eDNA-containing clones per library were next sequenced. All but one of the screened plasmids contained solely random noncoding eDNA sequences. The only exon-bearing vector encoded cyclophilin-type peptidyl-prolyl *cis-trans*-isomerase *CPR3* (orf19.1552).

**Functional matrix analysis.** The extracellular matrix has been shown to contribute to numerous biofilm functions (4, 5, 24, 25). In *C. albicans*, resistance to external threats, such as antifungals, is one clinically relevant role (13, 26, 27). A number of studies have shown that this biofilm component impedes drug penetration (9, 12, 28). Thus far, both a single matrix polysaccharide component,  $\beta$ -1,3-glucan, and eDNA have been linked to this process (9, 10, 13, 23). We utilized two sets of experiments to evaluate impedance and binding of the *C. albicans* biofilm matrix to the most commonly used antifungal, fluconazole. First, the location of radiolabeled fluconazole was determined in intact and matrix-deprived biofilms. As shown in Fig. 5A, the concentration of radiolabeled fluconazole measured within the intracellular space (containing the azole drug target) was 30% higher in the biofilms following partial matrix removal by gentle water bath sonication.

The antifungal drug binding of the *C. albicans* biofilm matrix was evaluated more specifically using one-dimensional  $^1\text{H}$  NMR analysis of fluconazole in the absence and presence of either total or individual matrix components. In these experiments, interaction of fluconazole with the matrix was evident by broadening of  $^1\text{H}$  peaks upon increasing concentrations of matrix (Fig. 5B). The spectral change was unsaturable across a wide range of matrix concentrations (Fig. 5C). In fact, the signal of both aromatic and azole protons broadened as a function of increasing concentra-

tions of the matrix, suggesting that the aromatic ring, as well as the doublet of heterocyclic azole rings of fluconazole, is interacting with matrix components. The lack of saturation is consistent with the binding participation of multiple matrix constituents with different affinity levels for fluconazole. Given the previously demonstrated role of  $\beta$ -1,3-glucan in the drug sequestration phenomenon, we explored binding with the purified carbohydrate fractions. Surprisingly, similar analysis with using the three purified carbohydrate fractions individually did not recapitulate the NMR interaction pattern of the full matrix complement (Fig. 5D). The fairly high concentration of matrix material required for NMR interaction studies unfortunately prohibited investigation of additional components in isolation or combination in the current investigation. However, we propose that matrix may have properties of an amalgam, in which multicomponent interactions yield emergent properties.

## DISCUSSION

The biofilm lifestyle represents a common form of microbial growth and persistence in nature (1, 29, 30). The microorganisms in a biofilm live in a self-produced extracellular matrix. The composition and function of this essential extracellular feature remain poorly understood for most microbes. To begin to explore this important topic, we have undertaken a comprehensive biochemical analysis of the extracellular matrix for the most common human fungal pathogen, *C. albicans*.

The compositions of the matrix in various microbial species have been shown to consist of complex mixtures of material from each of the four macromolecular classes: proteins, carbohydrates, lipids, and nucleic acid (4, 5, 30). Despite the frequent identification of these macromolecular constituents, it is clear there is enormous diversity in the composition and function of individual components among biofilm-forming organisms. Perhaps the single exception to this observation is the common identification of noncoding DNA, which appears to play both a structural and protective role (5, 23, 31). The present and previous investigations have similarly identified a modest amount of noncoding nucleic acid in the *C. albicans* matrix.

Exopolysaccharides have been shown to be a major component of most biofilm matrices (4, 24). For many organisms, a single matrix polysaccharide has been identified, while other organisms manufacture more than one matrix polysaccharide. For example, several prokaryotes appear to produce cellulose as the sole or predominant matrix sugar (4, 5). In scenarios where multiple matrix carbohydrates are observed, the construction of the individual polysaccharides is often environmentally dependent. *Pseudomonas aeruginosa*, for example, has been shown to produce three different polysaccharides, the Glc predominant Pel, the Man- and Gal-rich Psl, and uronic acid-containing alginate, depending upon the individual strain and clinical situation (32, 33). This is similar to most microbes where the building blocks are typically Glc or Man polymers and are variably independent polysaccharide units complexed with uronic acid or protein. Among fungal biofilms for which the matrix composition has been explored, the carbohydrate composition has been a complex with two or more components. Studies with both *Aspergillus fumigatus* and *Saccharomyces cerevisiae* analyses have identified both glucan- and mannan-containing materials (34, 35). The current investigation of *C. albicans* matrix identified carbohydrates as a major component. We detected three polysaccharides, all of which are similar to

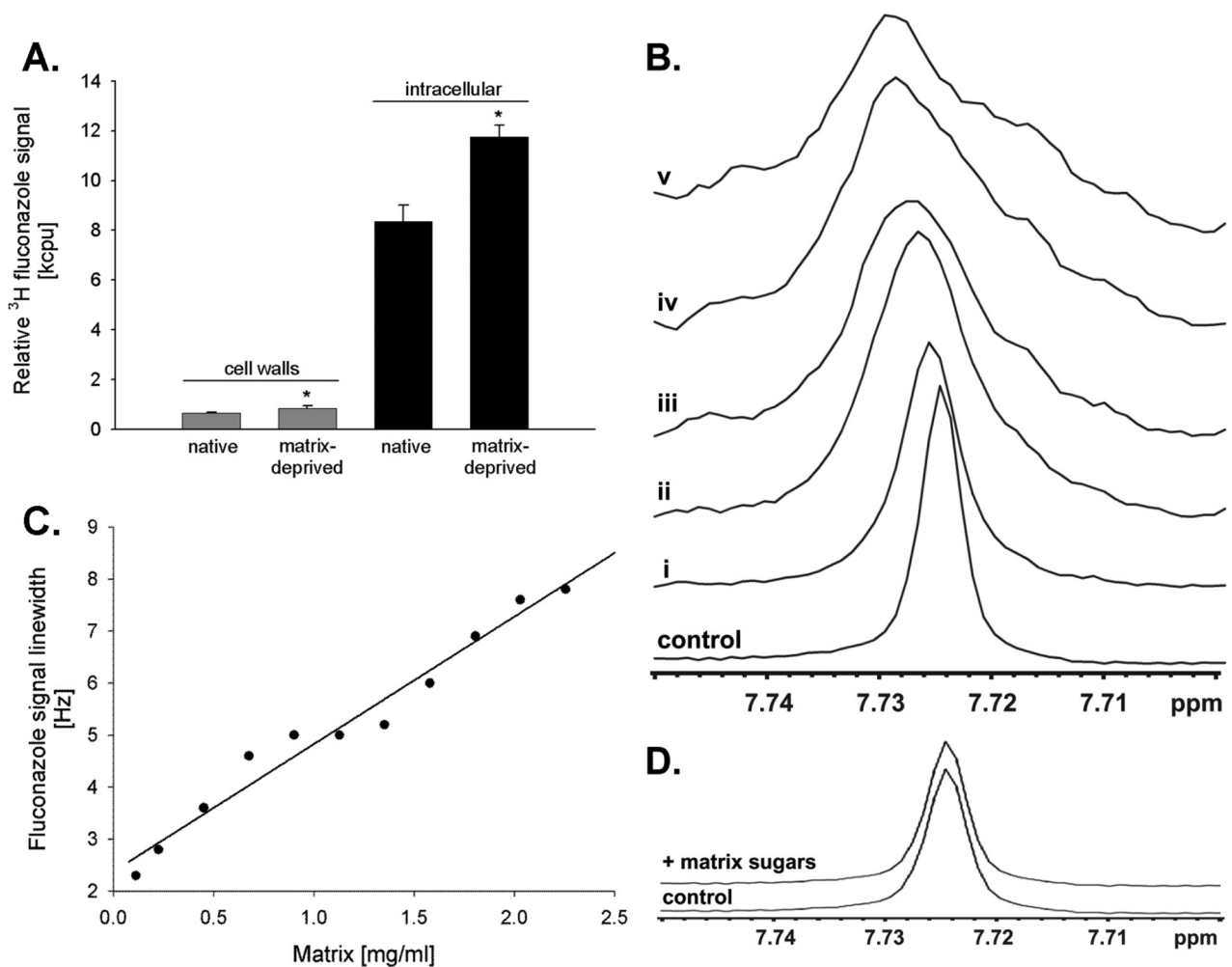


**FIG 5** Fluconazole sequestration and binding to the *C. albicans* biofilm extracellular matrix. (A) Sequestration of H3-labeled fluconazole in intact biofilms and matrix-deprived biofilms demonstrated a decreased accumulation of the drug intracellularly and in cell walls in intact biofilms containing the matrix. (B) Fluconazole interactions with the matrix studied by one-dimensional  $^1\text{H}$  NMR at 600 MHz determined as broadening of chemical shift peaks characteristic of protons present in the azole rings of fluconazole. Individual spectra correspond to the following matrix concentrations: (i) 0.11 mg/ml, (ii) 0.45 mg/ml, (iii) 1.28 mg/ml, (iv) 1.81 mg/ml, and (v) 2.26 mg/ml. (C) No binding saturation in the drug/matrix was observed, which suggests the participation of multiple matrix components with different affinity levels for fluconazole in this binding process. (D) No interactions between fluconazole and purified matrix glucomannan conjugates were identified, which suggests that either a combination of sugars or other nonsugar components in the matrix are responsible for drug sequestration.

key carbohydrate components of the *C. albicans* cell wall (36–38). The cell wall polysaccharide, chitin, was not identified in the matrix. Also, compared to the cell wall, the relative abundances of the matrix carbohydrates were different. Specifically, a unique branched-mannan- $\beta$ -1,6-glucan conjugate (MGCx) was the major matrix component, while in the cell wall,  $\beta$ -1,3-glucan was the predominant cell wall polysaccharide. This suggests that delivery or release of these matrix materials is not simply due to accumulation of released, intact cell wall.

Several lipid molecules have been found in the bacterial biofilm matrix. These have been shown to play roles in cell attachment and dispersion for these pathogens (39, 40). For example, the substituted fatty acid, *cis*-2-docecanoic acid, from *P. aeruginosa*, was found to induce cell dispersion from biofilms. A previous study of the lipid composition of the intact *C. albicans* biofilm identified a predominance of phosphatidylcholine (PC) and phosphatidylethanolamine (PE) (41). The current matrix analysis also identified

these constituents. However, the current matrix-specific exploration also found prostaglandin E2 (PGE<sub>2</sub>), a potent locally acting messenger molecule, as well as sphingolipids. Both have been shown to play vital roles in yeast biology; however, the role of these molecules in biofilm pathology remains unclear. A suggestion of importance in biofilm function is implied from studies examining the impact of PGE<sub>2</sub> inhibitors on *C. albicans* biofilms. Diclofenac exposure to biofilms was shown to reduce filamentation and potentiate the antifungal effect of an echinocandin (42, 43).

Proteins have been shown to represent a large portion of the biomass in most microbial matrix investigations (4, 5, 44). Proteins comprised more than half of the *C. albicans* matrix by weight in the current studies. The role of most of the microbial matrix complement remains unknown. The function of the majority of the proteome identified in other microbial systems suggests a structural or lectin role. Comparison of the current matrix proteome with intact *C. albicans* biofilm and biofilm supernatant

from a previous study identified a number of similarities, including an abundance of proteins involved in carbohydrate and amino acid metabolism (45, 46). We were surprised that we did not identify any *C. albicans* cell wall-associated proteins that have been shown promote biofilm adhesion and growth, such as the agglutinin-like sequence (ALS) family adhesins (47–49). This may be due to the relatively gentle matrix isolation process used. On the contrary, the putative function of most proteins from the current experiments is in the area of metabolism. This finding suggests the matrix may function as an external digestive system that breaks down extracellular biopolymers as an energy source. In fact, previous studies in bacterial biofilms have shown the matrix can be enzymatically active (50–54). We identified three glucan hydrolyzing enzymes that have been shown to deliver and potentially degrade matrix components (Xog1p, Bgl2p, Exg1p), which is consistent with this theory (13). The purpose of this enzymatic process is unclear but may serve to provide nutrition or detach cells for dispersion. Interestingly, many of the proteins identified in the *Candida* biofilm matrix do not contain defined secretion sequences. This suggests either a nonsecretion pathway, as has been postulated for other microbes, or the accumulation of proteins after cell death (55–57). Additional functional analyses will be important to discern the delivery and role of these matrix proteins.

We explored the clinical relevance of several of the *C. albicans* matrix components identified in the *in vitro* model by study in an animal biofilm infection model. Our previous studies discovered the secretion of  $\beta$ -1,3-glucan into the serum of animals with a vascular catheter biofilm. Similar study of a lung *Aspergillus* biofilm identified two polysaccharides, galactosaminogalactan and galactomannan (35). In the present study, we utilized microscopy of catheter biofilm infections to examine three matrix polysaccharides that were identified in the current *in vitro* studies. We found each of these polysaccharides ( $\beta$ -1,3-glucan,  $\beta$ -1,6-glucan, branched mannan) distributed in the extracellular milieu of the matrix of *C. albicans* biofilms in an animal central venous catheter biofilm. Proteomic analyses were also performed on the biofilm matrix collected from clinically relevant animal biofilm models. Sixteen similar *C. albicans* proteins were identified in both the *in vivo* and larger *in vitro* analysis. Most identified proteins represent components of carbohydrate and amino acid metabolic pathways. We were initially surprised to find only a small subset of *Candida* proteins within the *in vivo* data. In fact, the majority of proteins were from the animal host. We theorize this is due to the overwhelming amount of host material in the matrix. It also suggests the importance of host factors in matrix and biofilm formation. It is likely that consideration of host matrix components will be important to fully understand matrix function in this complex environment.

The aggregate matrix has been shown to include complexes of individual components, such as carbohydrate and protein (4, 5). Here, we describe two interacting matrix complex carbohydrate components, an MGCx. It is unclear whether the identified linear  $\beta$ -1,6-glucan was covalently bound to mannans, as no definitive NMR signal correlations were found. However, a relationship between the branched mannan and  $\beta$ -1,6-glucan was demonstrated by coseparation using both chromatographic techniques and a mannan-binding concanavalin A column, as well as colocalization by confocal microscopy (; data not shown). In fact, the secretion of water-insoluble  $\beta$ -1,6-glucan may be only possible as a result of its

tight physical interaction with highly branched and thereby water-soluble mannans. This kind of noncovalent “hooking” between polysaccharides has been recently proposed in *Candida glabrata* cell walls (19). However, the other possibility that  $\beta$ -1,6-glucan was directly linked to mannan cannot be excluded, as the NMR signal might be too weak to be detected, or the putative linkage may be through a noncarbohydrate linker, such as phosphate. In fact, Man-1-phosphate residues were detected in this study.

The heterogeneous nature of *Candida* biofilm matrix raises many questions about the roles that these different components play in the fitness of the biofilm. Previous studies have demonstrated a role for matrix in adhesion to surfaces, structural integrity, protection from external threats, signaling, and enzymatic activation of nutritional resources (4, 5, 58). Clearly, these functional questions have only begun to be addressed for many microbial biofilms. Arguably, the most clinically relevant phenotype of biofilm growth in the medical setting is resistance to antimicrobial therapy and the immune system (2, 59, 60). The mechanism underlying this phenotype is multifactorial (12, 23, 61, 62). Much of the observed drug resistance has been linked to impedance and even binding of anti-infectives to matrix components. For *C. albicans*, both the matrix polysaccharide,  $\beta$ -1,3-glucan, and extracellular DNA have been demonstrated to contribute to the drug resistance mechanism (11, 23, 28, 63). In the case of  $\beta$ -1,3-glucan, the presence of this constituent correlates with the ability of matrix to prevent penetration of antifungal drugs. The NMR results of the present study provide an additional line of evidence to support the importance of a matrix-drug interaction. The aggregate matrix and individual component NMR studies suggest the participation of more than a single *Candida* matrix constituent in this process. The identification of the functionally interacting matrix components is the focus of ongoing investigations.

## MATERIALS AND METHODS

***Candida* strains.** *C. albicans* K1 was used for all studies. The organism is a clinical isolate from a systemic biofilm *Candida* infection (64). See Text S1 in the supplemental material for detailed methods.

**Biofilm formation and matrix isolation.** A rolling bottle system was used to generate matrix for analyses. Briefly, aliquots of *C. albicans* grown in RPMI (RPMI 1640 buffered with morpholinepropanesulfonic acid [MOPS]) were used to inoculate a polystyrene roller bottle with a surface area of 850 cm<sup>2</sup> (Corning product number 3970). Bottles were placed on a roller apparatus (Wheaton Science Products, Millville, NJ), rolling at the rate of 20 rpm at 37°C. After 24 h, the biofilm culture medium was replaced and the bottles were incubated for another 24 h. After medium removal, the *C. albicans* biofilms were dislodged by spatula and gently sonicated to avoid cell wall disruption (42 kHz for 20 min [Branson 1510 Ultrasonic Cleaner sonicator] followed by sonication with a 1-cm by 5-cm probe in an Intrasonic Processor [Cole Parmer, Vernon Hills, IL] at an amplitude of 70 for 10 min). The aggregate biofilm was then centrifuged to separate fungal cells and matrix. The supernatant-containing matrix was then collected and lyophilized. The sample was resuspended in water and dialyzed (molecular weight cutoff of 3) for 5 consecutive days and again lyophilized yielding the “crude” biofilm matrix. Overall, a total of 700 bottles of the matrix corresponding to the biofilm area of 59.5 m<sup>2</sup> were collected for analysis. A similar cell mass of planktonic (nonbiofilm) *C. albicans* was collected and similarly processed to discern the impact of matrix processing on the cell wall.

**Carbohydrate analysis.** The carbohydrate concentration of crude matrix was determined colorimetrically (492 nm) using the phenol-sulfuric acid method (65). Structural analysis was performed after a purification and fractionation steps, including size exclusion chromatogra-

phy followed by separation on an anion exchanger HiPrep 16/10 DEAE FF column (GE Healthcare Life Sciences). Neutral free carbohydrates were collected in flowthrough fractions, which were pooled and applied to gel filtration on a HighPrep 16/60 Sephacryl S-300 HR column (GE Healthcare Life Sciences), yielding 22 individual polysaccharide peaks, F1 to F22. The molecular weight of biofilm matrix neutral carbohydrates was determined using size exclusion column calibration with a set of *Leuconostoc* species dextran standards (polymers with molecular weights [in thousands] of 100, 70, 40, 25, and 6).

Six carbohydrate fractions (F2, F5, F10, F14, F16, and F17) were examined by GC and NMR for monosugar and linkage analysis. First, matrix monosugar composition and quantification was performed on alditol acetate derivatives by GLC-FID (Shimadzu GC-2010 system; Shimadzu Co., Kyoto, Japan) (66). Next, 1D and 2D NMR spectroscopy was performed to complement monosugar assessment and to provide linkage analysis using a Bruker Biospin Avance III 500-MHz NMR spectrometer (Bruker BioSpin GmbH, Rheinstetten, Germany). One-dimensional spectra were collected using a standard one-pulse experiment. Two-dimensional, phase-sensitive, echo-antiecho  $^1\text{H}\{^{13}\text{C}\}$  HSQC spectra,  $^1\text{H}\{^1\text{H}\}$  NOESY spectra, echo-antiecho  $^1\text{H}\{^{13}\text{C}\}$  HSQC-TOCSY spectra, echo-antiecho  $^1\text{H}\{^{13}\text{C}\}$  HMBC spectra, and  $^1\text{H}\{^1\text{H}\}$  gradient-selected DQF-COSY spectra were also obtained. Next, complementary carbohydrate linkage analysis was undertaken on partially *O*-methylated alditol acetate derivatives by GC/mass spectrometry (MS) (67). Additionally, quantitative measurement of matrix  $\beta$ -1,3-glucan was also assessed for each carbohydrate chromatographic fraction using a Limulus lysate-based GlucateLL detection kit (Associates of Cape Cod, Massachusetts) (12, 68).

Small-angle X-ray scattering (SAXS) was used to gain further insight into the molecular size and shape of the most abundant mannan polysaccharide using a Bruker Nanostar benchtop system. Data were processed using the ATSAS software suite (69). GNOM was used to obtain pair distance distribution functions for each carbohydrate (70, 71).

To examine the location of matrix carbohydrates, biofilms were labeled with purified antibodies and imaged by confocal and electron microscopy. Biofilms were grown on sterile coverslips (Thermanox) for 24 h as previously described (13). Isolated matrix glucan and mannan components were used to raise monoclonal antibodies (MAbs) in mice (72). Individual clones recognizing branched mannan and  $\beta$ -1,6-glucan were selected for subsequent qualitative and quantitative matrix analyses (72). For confocal imaging, the mannan and  $\beta$ -1,6-glucan antibodies were fluorescently labeled with rhodamine and fluorescein isothiocyanate (FITC) (Pierce), respectively, and imaged on a Nikon A1R confocal microscope. Confocal images for FITC (excitation at 494 nm, emission at 517 nm) and rhodamine (excitation at 552 nm, emission at 575 nm) were obtained simultaneously using the Z-stack mode and processed for display using Nikon NIS-Elements Viewer version 3.2.

**Lipid analysis.** Lipids were extracted from the desalted lyophilized matrix powder with a mixture of  $\text{CHCl}_3$  and MeOH (2:1, by volume) as described elsewhere (73). Methylation of fatty acids was performed using 0.5 ml of 14%  $\text{BF}_3$  in MeOH, and methyl esters were recovered with hexane (74). Fatty acid methyl esters were analyzed by gas chromatography using a Hewlett-Packard 5890 (Hewlett-Packard, Palo Alto, CA) (74).

For prostaglandin analysis, the MeOH fraction from the initial  $\text{CHCl}_3$ -MeOH lipid extract was loaded on a preactivated SepPak classic  $\text{C}_{18}$  cartridge (Waters Corp., Milford, MA). Prostaglandins were eluted from the solid-phase extraction cartridge (Agilent ZORBAX 300SB,  $\text{C}_{18}$ , 1.8  $\mu\text{m}$ , 2.1 by 50 mm), chromatographically resolved on an Agilent 1200 high-performance liquid chromatography (HPLC) device (Agilent, Palo Alto, CA), and analyzed by mass spectrometry using an Agilent liquid chromatography (LC)/mass selective detector (MSD) time of flight (TOF) with electrospray ionization (negative-ion mode). Acquired data were processed and analyzed using the Analyst QS 1.1 build 9865 and Mass Hunter Qualitative Analysis software (Agilent, Palo Alto, CA).

Sterols (STs) were extracted and analyzed by Fast GC/MS as previously described (75). Spectroscopy was performed on a Shimadzu 2010 Plus

system equipped with a Shimadzu QP 2010 Ultra mass spectrometer detector, and mass spectra were compared with the standard mass spectra in the NIST MS library.

**Protein analysis.** The protein concentration of the crude matrix sample was assessed colorimetrically at 562 nm using the BCA protein assay kit (Pierce Biotechnology, Rockford, IL) (76). To identify specific proteins, trypsin-digested matrix was analyzed by nanoLC-MS/MS using an Agilent 1100 Nanoflow system (Agilent, Palo Alto, CA) connected to a hybrid linear ion trap-orbitrap mass spectrometer (LTQ-Orbitrap; Thermo, Fisher Scientific, San Jose, CA) equipped with a nanoelectrospray ion source (77). Raw MS/MS data were searched against a concatenated *C. albicans* amino acid sequence database using an in-house MASCOT search engine (78). Identified proteins were further annotated and filtered to a 1.5% peptide and 0.1% protein false discovery rate with Scaffold Q+ version 3.0 (Proteome Software Inc., Portland, OR) using the protein prophet algorithm (79). Functional mapping of the matrix proteome was performed using the KEGG database (80, 81).

**Nucleic acid analysis.** Nucleic acid concentrations were measured spectrophotometrically (260 nm) (82). To determine if the nucleic acid represented distinct coding regions, the *C. albicans* biofilm matrix nucleic acid was cloned and sequenced. Nucleotide sequences of eDNA were analyzed using the *Candida* Genome Database BLAST (83).

**In vivo matrix analysis.** The clinical relevance of select matrix components was explored using rodent biofilm models (84, 85). Following a 48-h biofilm formation phase, the implanted medical devices were removed and processed for gel-free proteomics and for microscopy to analyze and localize matrix carbohydrates. Monoclonal antibodies to each of the two major matrix polysaccharides,  $\alpha$ -1,2 branched  $\alpha$ -1,6-mannan and  $\beta$ -1,6-glucan, were used for confocal imaging as described above. For transmission electron microscopy (TEM),  $\beta$ -1,3-glucan antibodies were linked to Nanogold particles and used for labeling *in vivo* biofilms. After catheter removal, biofilms were collected and prepared for immunogold TEM. Briefly, catheter biofilms were dislodged, fixed, embedded, treated with Aurion rabbit-gold conjugate-blocking solution, exposed to the primary  $\beta$ -1,3-glucan antibody for 1 day, rinsed, and then exposed to a secondary antibody (Aurion rabbit anti-goat IgG gold conjugate; 1:25 dilution). Following washing and postfixation, samples were observed with a Philips CM120 transmission electron microscope equipped with a SIS MEGA-VIEW III digital camera and analyzed using SIS analysis software.

**Functional matrix analysis.** We utilized H3-labeled fluconazole to assess biofilm and matrix sequestration before and after matrix removal. Briefly, biofilms were grown for 48 h and washed. For a subset of biofilms, the matrix was removed by sonication. Biofilms were treated with H3-labeled fluconazole and chased with nonradioactive drug. Biofilms were washed, dislodged, and collected. The matrix was removed by vortexing and centrifugation. Radiolabeled drug in the total and each biofilm component was measured by liquid scintillation counting (TRI-CARB 2100 TR; Packard). Data were normalized for biofilm dry cell weight.

Interactions between the biofilm matrix and fluconazole were also probed by using a one-dimensional  $^1\text{H}$  NMR Bruker Biospin Avance III 600-MHz NMR spectrometer (Bruker BioSpin GmbH) equipped with a 1.7-mm triple resonance, cryogenic probe, CPTXI 500 H-C/N-D (86, 87). The approach was based on monitoring chemical shifts of fluconazole-specific protons in the absence and presence of the biofilm matrix (88).

## SUPPLEMENTAL MATERIAL

Supplemental material for this article may be found at <http://mbio.asm.org/lookup/suppl/doi:10.1128/mBio.01333-14/-/DCSupplemental>.

Text S1, DOCX file, 0.1 MB.

Figure S1, TIF file, 0.6 MB.

Figure S2, TIF file, 6.1 MB.

Table S1, DOCX file, 0.1 MB.

Table S2, DOCX file, 0.1 MB.

Table S3, DOCX file, 0.1 MB.

Table S4, DOCX file, 0.1 MB.

## ACKNOWLEDGMENTS

The studies were funded by NIH R01 AI073289. We thank Christian Heiss and Parastoo Azadi for their invaluable help with NMR data interpretation that in part was funded by the NIH/NCRR Resource for Integrated Glycotechnology at the University of Georgia (P41RR005351). This study made use of the National Magnetic Resonance Facility at Madison, which is supported by NIH grants P41RR02301 (BRTP/NCRR) and P41GM10399 (NIGMS). Additional equipment was purchased with funds from the University of Wisconsin, the NIH (RR02781, RR08438), the NSF (DMB-8415048, OIA-9977486, BIR-9214394), the DOE, and the USDA. Small angle X-ray scattering (SAXS) equipment was purchased with funds from NIH grant S10RR027000 (NCRR).

We also thank Grzegorz Sabat for his excellent technical assistance with spectral analyses.

## REFERENCES

- Costerton JW, Stewart PS, Greenberg EP. 1999. Bacterial biofilms: a common cause of persistent infections. *Science* 284:1318–1322. <http://dx.doi.org/10.1126/science.284.5418.1318>.
- Donlan RM, Costerton JW. 2002. Biofilms: survival mechanisms of clinically relevant microorganisms. *Clin. Microbiol. Rev.* 15:167–193. <http://dx.doi.org/10.1128/CMR.15.2.167-193.2002>.
- Potera C. 1999. Forging a link between biofilms and disease. *Science* 283:1837–1839. <http://dx.doi.org/10.1126/science.283.5409.1837>.
- Branda SS, Vik S, Friedman L, Kolter R. 2005. Biofilms: the matrix revisited. *Trends Microbiol.* 13:20–26. <http://dx.doi.org/10.1016/j.tim.2004.11.006>.
- Flemming HC, Wingender J. 2010. The biofilm matrix. *Nat. Rev. Microbiol.* 8:623–633.
- Douglas LJ. 2003. *Candida* biofilms and their role in infection. *Trends Microbiol.* 11:30–36. [http://dx.doi.org/10.1016/S0966-842X\(02\)00002-1](http://dx.doi.org/10.1016/S0966-842X(02)00002-1).
- Pfaller MA, Diekema DJ. 2007. Epidemiology of invasive candidiasis: a persistent public health problem. *Clin. Microbiol. Rev.* 20:133–163. <http://dx.doi.org/10.1128/CMR.00029-06>.
- Al-Fattani MA, Douglas LJ. 2004. Penetration of *Candida* biofilms by antifungal agents. *Antimicrob. Agents Chemother.* 48:3291–3297. <http://dx.doi.org/10.1128/AAC.48.9.3291-3297.2004>.
- Vediyappan G, Rossignol T, d'Enfert C. 2010. Interaction of *Candida albicans* biofilms with antifungals: transcriptional response and binding of antifungals to beta-glucans. *Antimicrob. Agents Chemother.* 54:2096–2111. <http://dx.doi.org/10.1128/AAC.01638-09>.
- Nett JE, Sanchez H, Cain MT, Andes DR. 2010. Genetic basis of *Candida* biofilm resistance due to drug-sequestering matrix glucan. *J. Infect. Dis.* 202:171–175. <http://dx.doi.org/10.1093/infdis/jiq1200>.
- Nett JE, Crawford K, Marchillo K, Andes DR. 2010. Role of Fks1p and matrix glucan in *Candida albicans* biofilm resistance to an echinocandin, pyrimidine, and polyene. *Antimicrob. Agents Chemother.* 54:3505–3508. <http://dx.doi.org/10.1128/AAC.00227-10>.
- Nett J, Lincoln L, Marchillo K, Massey R, Holoyda K, Hoff B, Van-Handel M, Andes D. 2007. Putative role of beta-1,3 glucans in *Candida albicans* biofilm resistance. *Antimicrob. Agents Chemother.* 51:510–520. <http://dx.doi.org/10.1128/AAC.01056-06>.
- Taff HT, Nett JE, Zarnowski R, Ross KM, Sanchez H, Cain MT, Hamaker J, Mitchell AP, Andes DR. 2012. A *Candida* biofilm-induced pathway for matrix glucan delivery: implications for drug resistance. *PLoS Pathog.* 8:e1002848. <http://dx.doi.org/10.1371/journal.ppat.1002848>.
- Nobile CJ, Nett JE, Hernday AD, Homann OR, Deneault JS, Nantel A, Andes DR, Johnson AD, Mitchell AP. 2009. *Biofilm matrix* regulation by *Candida albicans* Zap1. *PLoS Biol.* 7:e1000133. <http://dx.doi.org/10.1371/journal.pbio.1000133>.
- Shibata N, Kobayashi H, Okawa Y, Suzuki S. 2003. Existence of novel beta-1,2 linkage-containing side chain in the mannan of *Candida lusitanae*, antigenically related to *Candida albicans* serotype A. *Eur. J. Biochem.* 270:2565–2575. <http://dx.doi.org/10.1046/j.1432-1033.2003.03622.x>.
- Shibata N, Okawa Y. 2010. Conformational analysis of beta-1,2-linked manno-1,6-bisphosphate, specific antigen of pathogenic yeast *Candida albicans*. *Chem. Pharm. Bull.* 58:1386–1390. <http://dx.doi.org/10.1248/cpb.58.1386>.
- Shibata N, Suzuki A, Kobayashi H, Okawa Y. 2007. Chemical structure of the cell wall mannan of *Candida albicans* serotype A and its difference in yeast and hyphal forms. *Biochem. J.* 404:365–372. <http://dx.doi.org/10.1042/BJ20070081>.
- Lowman DW, West LJ, Bearden DW, Wempe MF, Power TD, Ensley HE, Haynes K, Williams DL, Kruppa MD. 2011. New insights into the structure of (1→3,1→6)-beta-D-glucan side chains in the *Candida glabrata* cell wall. *PLoS One* 6:e27614. <http://dx.doi.org/10.1371/journal.pone.0027614>.
- Lowman DW, Ensley HE, Greene RR, Knagge KJ, Williams DL, Kruppa MD. 2011. Mannan structural complexity is decreased when *Candida albicans* is cultivated in blood or serum at physiological temperature. *Carbohydr. Res.* 346:2752–2759. <http://dx.doi.org/10.1016/j.carres.2011.09.029>.
- Takahashi S, Kudoh A, Okawa Y, Shibata N. 2012. Significant differences in the cell wall mannans from three *Candida glabrata* strains correlate with antifungal drug sensitivity. *FEBS J.* 279:1844–1856. <http://dx.doi.org/10.1111/j.1742-4658.2012.08564.x>.
- Bernhardt JFS, Hecker M, Siebourg J. 2009. Visualizing gene expression data via Voronoi treemaps, p 233–241. *In* Sixth International Symposium on Voronoi diagrams. IEEE, Piscataway, NJ. <http://dx.doi.org/10.1109/ISVD.2009.33>.
- Peltroche-Llacsahuanga H, Goyard S, d'Enfert C, Prill SK, Ernst JF. 2006. Protein O-mannosyltransferase isoforms regulate biofilm formation in *Candida albicans*. *Antimicrob. Agents Chemother.* 50:3488–3491. <http://dx.doi.org/10.1128/AAC.00606-06>.
- Martins M, Uppuluri P, Thomas DP, Cleary IA, Henriques M, Lopez-Ribot JL, Oliveira R. 2010. Presence of extracellular DNA in the *Candida albicans* biofilm matrix and its contribution to biofilms. *Mycopathologia* 169:323–331. <http://dx.doi.org/10.1007/s11046-009-9264-y>.
- Flemming HC, Neu TR, Wozniak DJ. 2007. The EPS matrix: the “house of biofilm cells.” *J. Bacteriol.* 189:7945–7947. <http://dx.doi.org/10.1128/JB.00858-07>.
- Mah TF, Pitts B, Pellock B, Walker GC, Stewart PS, O'Toole GA. 2003. A genetic basis for *Pseudomonas aeruginosa* biofilm antibiotic resistance. *Nature* 426:306–310. <http://dx.doi.org/10.1038/nature02122>.
- Al-Fattani MA, Douglas LJ. 2006. Biofilm matrix of *Candida albicans* and *Candida tropicalis*: chemical composition and role in drug resistance. *J. Med. Microbiol.* 55:999–1008. <http://dx.doi.org/10.1099/jmm.0.46569-0>.
- Kojic EM, Darouiche RO. 2004. *Candida* infections of medical devices. *Clin. Microbiol. Rev.* 17:255–267. <http://dx.doi.org/10.1128/CMR.17.2.255-267.2004>.
- Robbins N, Uppuluri P, Nett J, Rajendran R, Ramage G, Lopez-Ribot JL, Andes D, Cowen LE. 2011. Hsp90 governs dispersion and drug resistance of fungal biofilms. *PLoS Pathog.* 7:e1002257. <http://dx.doi.org/10.1371/journal.ppat.1002257>.
- Donlan RM. 2001. Biofilm formation: a clinically relevant microbiological process. *Clin. Infect. Dis.* 33:1387–1392. <http://dx.doi.org/10.1086/322972>.
- O'Toole GA. 2003. To build a biofilm. *J. Bacteriol.* 185:2687–2689. <http://dx.doi.org/10.1128/JB.185.9.2687-2689.2003>.
- Rajendran R, Williams C, Lappin DF, Millington O, Martins M, Ramage G. 2013. Extracellular DNA release acts as an antifungal resistance mechanism in mature *Aspergillus fumigatus* biofilms. *Eukaryot. Cell* 12:420–429. <http://dx.doi.org/10.1128/EC.00287-12>.
- Colvin KM, Gordon VD, Murakami K, Borlee BR, Wozniak DJ, Wong GC, Parsek MR. 2011. The Pel polysaccharide can serve a structural and protective role in the biofilm matrix of *Pseudomonas aeruginosa*. *PLoS Pathog.* 7:e1001264. <http://dx.doi.org/10.1371/journal.ppat.1001264>.
- Colvin KM, Irie Y, Tart CS, Urbano R, Whitney JC, Ryder C, Howell PL, Wozniak DJ, Parsek MR. 2012. The Pel and Psl polysaccharides provide *Pseudomonas aeruginosa* structural redundancy within the biofilm matrix. *Environ. Microbiol.* 14:1913–1928. <http://dx.doi.org/10.1111/j.1462-2920.2011.02657.x>.
- Beauvais A, Lousert C, Prevost MC, Verstrepen K, Latgé JP. 2009. Characterization of a biofilm-like extracellular matrix in FLO1-expressing *Saccharomyces cerevisiae* cells. *FEMS Yeast Res.* 9:411–419. <http://dx.doi.org/10.1111/j.1567-1364.2009.00482.x>.
- Lousert C, Schmitt C, Prevost MC, Balloy V, Fadel E, Philippe B, Kauffmann-Lacroix C, Latgé JP, Beauvais A. 2010. *In vivo* biofilm composition of *Aspergillus fumigatus*. *Cell. Microbiol.* 12:405–410. <http://dx.doi.org/10.1111/j.1462-5822.2009.01409.x>.
- Chaffin WL, López-Ribot JL, Casanova M, Gosalbo D, Martínez JP. 1998. Cell wall and secreted proteins of *Candida albicans*: identification, function, and expression. *Microbiol. Mol. Biol. Rev.* 62:130–180.

37. Kapteyn JC, Hoyer LL, Hecht JE, Müller WH, Andel A, Verkleij AJ, Makarow M, Van Den Ende H, Klis FM. 2000. The cell wall architecture of *Candida albicans* wild-type cells and cell wall-defective mutants. *Mol. Microbiol.* 35:601–611.
38. Klis FM, de Groot P, Hellingwerf K. 2001. Molecular organization of the cell wall of *Candida albicans*. *Med. Mycol.* 39(Suppl 1):1–8. <http://dx.doi.org/10.1080/744118879>.
39. Davies DG, Marques CN. 2009. A fatty acid messenger is responsible for inducing dispersion in microbial biofilms. *J. Bacteriol.* 191:1393–1403. <http://dx.doi.org/10.1128/JB.01214-08>.
40. Davey ME, Caiazza NC, O'Toole GA. 2003. Rhamnolipid surfactant production affects biofilm architecture in *Pseudomonas aeruginosa* PAO1. *J. Bacteriol.* 185:1027–1036. <http://dx.doi.org/10.1128/JB.185.3.1027-1036.2003>.
41. Lattif AA, Mukherjee PK, Chandra J, Roth MR, Welti R, Rouabhia M, Ghannoum MA. 2011. Lipidomics of *Candida albicans* biofilms reveals phase-dependent production of phospholipid molecular classes and role for lipid rafts in biofilm formation. *Microbiology* 157:3232–3242. <http://dx.doi.org/10.1099/mic.0.051086-0>.
42. Bink A, Kuchariková S, Neirinck B, Vleugels J, Van Dijck P, Cammue BP, Thevissen K. 2012. The nonsteroidal anti-inflammatory drug diclofenac potentiates the *in vivo* activity of caspofungin against *Candida albicans* biofilms. *J. Infect. Dis.* 206:1790–1797. <http://dx.doi.org/10.1093/infdis/jis594>.
43. Ghalehnoo ZR, Rashki A, Najimi M, Dominguez A. 2010. The role of diclofenac sodium in the dimorphic transition in *Candida albicans*. *Microb. Pathog.* 48:110–115. <http://dx.doi.org/10.1016/j.micpath.2009.12.003>.
44. Branda SS, Chu F, Kearns DB, Losick R, Kolter R. 2006. A major protein component of the *Bacillus subtilis* biofilm matrix. *Mol. Microbiol.* 59:1229–1238. <http://dx.doi.org/10.1111/j.1365-2958.2005.05020.x>.
45. Thomas DP, Bachmann SP, Lopez-Ribot JL. 2006. Proteomics for the analysis of the *Candida albicans* biofilm lifestyle. *Proteomics* 6:5795–5804. <http://dx.doi.org/10.1002/pmic.200600332>.
46. Martínez-Gomariz M, Perumal P, Mekala S, Nombela C, Chaffin WL, Gil C. 2009. Proteomic analysis of cytoplasmic and surface proteins from yeast cells, hyphae, and biofilms of *Candida albicans*. *Proteomics* 9:2230–2252. <http://dx.doi.org/10.1002/pmic.200700594>.
47. Nobile CJ, Andes DR, Nett JE, Smith FJ, Yue F, Phan QT, Edwards JE, Filler SG, Mitchell AP. 2006. Critical role of Bcr1-dependent adhesins in *C. albicans* biofilm formation *in vitro* and *in vivo*. *PLoS Pathog.* 2:e63. <http://dx.doi.org/10.1371/journal.ppat.0020063>.
48. Nobile CJ, Mitchell AP. 2005. Regulation of cell-surface genes and biofilm formation by the *C. albicans* transcription factor Bcr1p. *Curr. Biol.* 15:1150–1155. <http://dx.doi.org/10.1016/j.cub.2005.05.047>.
49. Liu Y, Filler SG. 2011. *Candida albicans* Als3, a multifunctional adhesin and invasin. *Eukaryot. Cell* 10:168–173. <http://dx.doi.org/10.1128/EC.00279-10>.
50. Sutherland IW. 2001. The biofilm matrix—an immobilized but dynamic microbial environment. *Trends Microbiol.* 9:222–227. [http://dx.doi.org/10.1016/S0966-842X\(01\)02012-1](http://dx.doi.org/10.1016/S0966-842X(01)02012-1).
51. Absalon C, Ymele-Leki P, Watnick PI. 2012. The bacterial biofilm matrix as a platform for protein delivery. *mBio* 3(4):. <http://dx.doi.org/10.1128/mBio.00127-12e00127-00112>.
52. Romani AM, Fund K, Artigas J, Schwartz T, Sabater S, Obst U. 2008. Relevance of polymeric matrix enzymes during biofilm formation. *Microb. Ecol.* 56:427–436. <http://dx.doi.org/10.1007/s00248-007-9361-8>.
53. Jiao Y, D'Haeseleer P, Dill BD, Shah M, Verberkmoes NC, Hettich RL, Banfield JF, Thelen MP. 2011. Identification of biofilm matrix-associated proteins from an acid mine drainage microbial community. *Appl. Environ. Microbiol.* 77:5230–5237. <http://dx.doi.org/10.1128/AEM.03005-10>.
54. Chen C, Krishnan V, Macon K, Manne K, Narayana SV, Schneewind O. 2013. Secreted proteases control autolysin-mediated biofilm growth of *Staphylococcus aureus*. *J. Biol. Chem.* 288:29440–29452. <http://dx.doi.org/10.1074/jbc.M113.502039>.
55. Nosanchuk JD, Nimrichter L, Casadevall A, Rodrigues ML. 2008. A role for vesicular transport of macromolecules across cell walls in fungal pathogenesis. *Commun. Integr. Biol.* 1:37–39. <http://dx.doi.org/10.4161/cib.1.1.6639>.
56. Nombela C, Gil C, Chaffin WL. 2006. Non-conventional protein secretion in yeast. *Trends Microbiol.* 14:15–21. <http://dx.doi.org/10.1016/j.tim.2005.11.009>.
57. Nickel W, Rabouille C. 2009. Mechanisms of regulated unconventional protein secretion. *Nat. Rev. Mol. Cell Biol.* 10:148–155. <http://dx.doi.org/10.1038/nrm2617>.
58. Sutherland I. 2001. Biofilm exopolysaccharides: a strong and sticky framework. *Microbiology* 147:3–9.
59. Ramage G, Rajendran R, Sherry L, Williams C. 2012. Fungal biofilm resistance. *Int. J. Microbiol.* 2012:528521. <http://dx.doi.org/10.1155/2012/528521>.
60. Mah TF, O'Toole GA. 2001. Mechanisms of biofilm resistance to antimicrobial agents. *Trends Microbiol.* 9:34–39. [http://dx.doi.org/10.1016/S0966-842X\(00\)01913-2](http://dx.doi.org/10.1016/S0966-842X(00)01913-2).
61. Mukherjee PK, Chandra J, Kuhn DM, Ghannoum MA. 2003. Mechanism of fluconazole resistance in *Candida albicans* biofilms: phase-specific role of efflux pumps and membrane sterols. *Infect. Immun.* 71:4333–4340. <http://dx.doi.org/10.1128/IAI.71.8.4333-4340.2003>.
62. Ramage G, Bachmann S, Patterson TF, Wickes BL, López-Ribot JL. 2002. Investigation of multidrug efflux pumps in relation to fluconazole resistance in *Candida albicans* biofilms. *J. Antimicrob. Chemother.* 49:973–980. <http://dx.doi.org/10.1093/jac/dfk049>.
63. Martins M, Henriques M, Lopez-Ribot JL, Oliveira R. 2012. Addition of DNase improves the *in vitro* activity of antifungal drugs against *Candida albicans* biofilms. *Mycoses* 55:80–85. <http://dx.doi.org/10.1111/j.1439-0507.2011.02047.x>.
64. Andes D, van Ogtrop M. 1999. Characterization and quantitation of the pharmacodynamics of fluconazole in a neutropenic murine disseminated candidiasis infection model. *Antimicrob. Agents Chemother.* 43:2116–2120.
65. Dubois M, Gilles K, Hamilton JK, Rebers PA, Smith F. 1951. A colorimetric method for the determination of sugars. *Nature* 168:167. <http://dx.doi.org/10.1038/168167b0>.
66. Henry RJ, Blakeney AB, Harris PJ, Stone BA. 1983. Detection of neutral and aminosugars from glycoproteins and polysaccharides as their alditol acetates. *J. Chromatogr.* 256:419–427. [http://dx.doi.org/10.1016/S0021-9673\(01\)88259-5](http://dx.doi.org/10.1016/S0021-9673(01)88259-5).
67. Sassaki GL, Gorin PA, Souza LM, Czelusniak PA, Iacomini M. 2005. Rapid synthesis of partially O-methylated alditol acetate standards for GC-MS: some relative activities of hydroxyl groups of methyl glycopyranosides on Purdie methylation. *Carbohydr. Res.* 340:731–739. <http://dx.doi.org/10.1016/j.carres.2005.01.020>.
68. Nett J, Lincoln L, Marchillo K, Andes D. 2007. Beta-1,3 glucan as a test for central venous catheter biofilm infection. *J. Infect. Dis.* 195:1705–1712. <http://dx.doi.org/10.1086/517522>.
69. Petoukhov MV, Svergun DI. 2013. Applications of small-angle X-ray scattering to biomacromolecular solutions. *Int. J. Biochem. Cell Biol.* 45:429–437. <http://dx.doi.org/10.1016/j.biocel.2012.10.017>.
70. König S, Svergun D, Koch MH, Hübner G, Schellenberger A. 1992. Synchrotron radiation solution X-ray scattering study of the pH dependence of the quaternary structure of yeast pyruvate decarboxylase. *Biochemistry* 31:8726–8731. <http://dx.doi.org/10.1021/bi00152a007>.
71. Van Le B, Franke D, Svergun DI, Han T, Hwang HY, Kim KK. 2009. Structural and functional characterization of soluble endoglin receptor. *Biochem. Biophys. Res. Commun.* 383:386–391. <http://dx.doi.org/10.1016/j.bbrc.2009.02.162>.
72. Yokoyama WM. 2001. Production of monoclonal antibodies. *Curr. Protocols Immunol.* 2:II:2.5. <http://dx.doi.org/10.1002/0471142735.im0205s03>.
73. Zarnowski R, Jaromin A, Certik M, Czabany T, Fontaine J, Jakubik T, Iqbal MC, Grandmougin-Ferjani A, Kozubek A, Pietr SJ. 2004. The oil of *Adenantha pavonina* L. seeds and its emulsions. *Z. Naturforsch. C* 59:321–326.
74. Zarnowski R, Connolly PA, Wheat LJ, Woods JP. 2007. Production of extracellular proteolytic activity by *Histoplasma capsulatum* grown in *Histoplasma*-macrophage medium is limited to restriction fragment length polymorphism class 1 isolates. *Diagn. Microbiol. Infect. Dis.* 59:39–47. <http://dx.doi.org/10.1016/j.diagmicrobio.2007.03.020>.
75. Zarnowski R, Ellis RJ, Lewicka T, Pietr SJ. 2004. Effect of age on the fatty acid composition of the *Bacillus subtilis* PO270 isolated from wheat rhizosphere. *Pol. J. Microbiol.* 53:267–272.
76. Smith PK, Krohn RI, Hermanson GT, Mallia AK, Gartner FH, Provenzano MD, Fujimoto EK, Goetze NM, Olson BJ, Klenk DC. 1985. Measurement of protein using bicinchoninic acid. *Anal. Biochem.* 150:76–85. [http://dx.doi.org/10.1016/0003-2697\(85\)90442-7](http://dx.doi.org/10.1016/0003-2697(85)90442-7).
77. Martin SE, Shabanowitz J, Hunt DF, Marto JA. 2000. Subfemtomole MS and MS/MS peptide sequence analysis using nano-HPLC micro-ESI Fou-

- rier transform ion cyclotron resonance mass spectrometry. *Anal. Chem.* 72:4266–4274. <http://dx.doi.org/10.1021/ac000497v>.
78. Perkins DN, Pappin DJ, Creasy DM, Cottrell JS. 1999. Probability-based protein identification by searching sequence databases using mass spectrometry data. *Electrophoresis* 20:3551–3567. [http://dx.doi.org/10.1002/\(SICI\)1522-2683\(19991201\)20:18<3551::AID-ELPS3551>3.0.CO;2-2](http://dx.doi.org/10.1002/(SICI)1522-2683(19991201)20:18<3551::AID-ELPS3551>3.0.CO;2-2).
  79. Keller A, Nesvizhskii AI, Kolker E, Aebersold R. 2002. Empirical statistical model to estimate the accuracy of peptide identifications made by MS/MS and database search. *Anal. Chem.* 74:5383–5392. <http://dx.doi.org/10.1021/ac025747h>.
  80. Kanehisa M, Goto S. 2000. KEGG: Kyoto encyclopedia of genes and genomes. *Nucleic Acids Res.* 28:27–30. <http://dx.doi.org/10.1093/nar/28.7.e27>.
  81. Kanehisa M, Goto S, Sato Y, Furumichi M, Tanabe M. 2012. KEGG for integration and interpretation of large-scale molecular data sets. *Nucleic Acids Res.* 40:D109–D114. <http://dx.doi.org/10.1093/nar/gkr988>.
  82. Sandhu LC, Warters RL, Dethlefsen LA. 1985. Fluorescence studies of Hoechst 33342 with supercoiled and relaxed plasmid pBR322 DNA. *Cytometry* 6:191–194. <http://dx.doi.org/10.1002/cyto.990060304>.
  83. Inglis DO, Arnaud MB, Binkley J, Shah P, Skrzypek MS, Wymore F, Binkley G, Miyasato SR, Simison M, Sherlock G. 2012. The *Candida* genome database incorporates multiple *Candida* species: multispecies search and analysis tools with curated gene and protein information for *Candida albicans* and *Candida glabrata*. *Nucleic Acids Res.* 40: D667–D674. <http://dx.doi.org/10.1093/nar/gkr945>.
  84. Andes D, Nett J, Oschel P, Albrecht R, Marchillo K, Pitula A. 2004. Development and characterization of an *in vivo* central venous catheter *Candida albicans* biofilm model. *Infect. Immun.* 72:6023–6031. <http://dx.doi.org/10.1128/IAI.72.10.6023-6031.2004>.
  85. Nett JE, Marchillo K, Spiegel CA, Andes DR. 2010. Development and validation of an *in vivo* *Candida albicans* biofilm denture model. *Infect. Immun.* 78:3650–3659. <http://dx.doi.org/10.1128/IAI.00480-10>.
  86. Hwang TL, Shaka AJ. 1998. Multiple-pulse mixing sequences that selectively enhance chemical exchange or cross-relaxation peaks in high-resolution NMR spectra. *J. Magn. Reson.* 135:280–287. <http://dx.doi.org/10.1006/jmre.1998.1598>.
  87. Hwang T, Shaka AJ. 1995. Water suppression that works. Excitation sculpting using arbitrary wave-forms and pulse-field gradients. *J. Magn. Reson.* 112:275–279. <http://dx.doi.org/10.1006/jmra.1995.1047>.
  88. Dalvit C, Flocco M, Veronesi M, Stockman BJ. 2002. Fluorine-NMR competition binding experiments for high-throughput screening of large compound mixtures. *Comb. Chem. High Throughput Screen.* 5:605–611. <http://dx.doi.org/10.2174/1386207023329923>.